Ultrasmooth, Highly Spherical Monocrystalline Gold Particles for Precision Plasmonics

Permanent link

http://nrs.harvard.edu/urn-3:HUL.InstRepos:24902804

Share Your Story

The Harvard community has made this article openly available.
Please share how this access benefits you. Submit a story.

Accessibility

Ultra-Smooth, Highly Spherical Monocrystalline Gold Particles for Precision Plasmonics

You-Jin Lee,[†, ‡ ,+] Nicholas B. Schade,[§,+] Li Sun,[⊥,+] Jonathan A. Fan,[#] Doo Ri Bae,[‡] Marcelo M. Mariscal,[¶] Gaehang Lee,[‡,*] Federico Capasso,[⊥] Stefano Sacanna,[∥] Vinothan N. Manoharan,[⊥,§] Gi-Ra Yi[†,*]

[†]Department of Polymer Science and Engineering and School of Chemical Engineering, Sungkyunkwan University, Suwon 440-746, Republic of Korea

[‡]Division of Materials Science, Korea Basic Science Institute, Daejeon 305-806, Republic of Korea

[§]Department of Physics, Harvard University, Cambridge MA 02138 USA

[⊥]School of Engineering and Applied Sciences, Harvard University, Cambridge MA 02138 USA

[#]Beckman Institute, University of Illinois, 405 North Mathews Avenue, Urbana, IL 61801 USA

[¶]INFIQC/CONICET, Departamento de Matemática y Física, Facultad de Ciencias Químicas, Universidad Nacional de Córdoba, XUA5000 Córdoba, Argentina

[∥]Molecular Design Institute, Department of Chemistry, New York University, New York, NY 10003 USA

[+]These authors contributed equally to this work

[*]To whom correspondence should be addressed: yigira@skku.edu, ghlee@kbsi.re.kr

ABSTRACT

Ultra-smooth, highly spherical monocrystalline gold particles were prepared by a cyclic process of slow growth followed by slow chemical etching, which selectively removes edges and vertices. The etching process effectively makes the surface tension isotropic, so that spheres are favored under quasi-static conditions. It is scalable up to particle sizes of 200 nm or more. The resulting spherical crystals display uniform scattering spectra and consistent optical coupling at small separations, even showing Fano-like resonances in small clusters. The high monodispersity of the particles we demonstrate should facilitate the self-assembly of nanoparticle clusters with uniform optical resonances, which could in turn be used to fabricate optical metafluids. Narrow size distributions are required not only to control the spectral features, but also the morphology and yield of clusters in certain assembly schemes.

KEYWORDS: Gold nanospheres, plasmonics, monodisperse, chemical etching, Fano-like resonance.

TOC Graphic
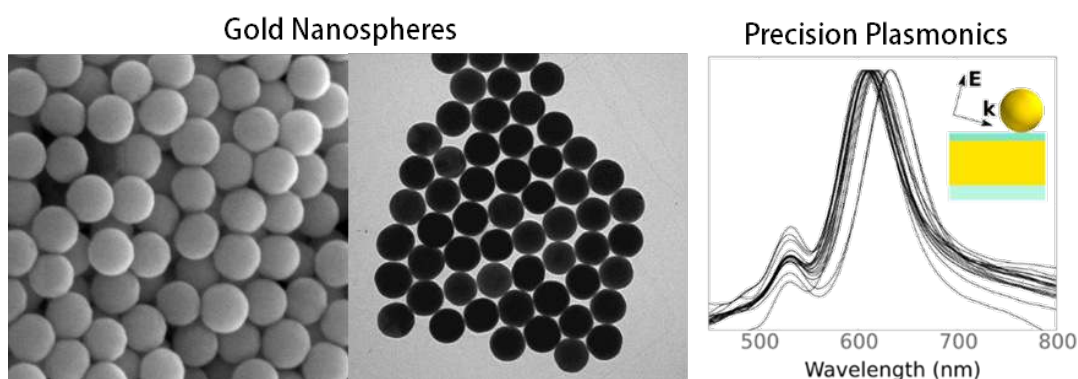
In equilibrium, a nanoscale crystal adopts a polyhedral morphology to minimize its surface free energy. As a result, metallic nanoparticles grown near equilibrium form facets.[1–3] Although the plasmon resonances and ease of functionalization[4] make such particles promising[1] for bottom-up assembly of optical resonators[5,6] and isotropic metamaterials,[7] it is difficult to make structures whose optical properties are reproducible from one particle or one multiple-particle cluster to the next since the resonances are often sensitive to features such as sharp corners,[8] number of facets,[9] roughness,[10] and overall size and shape.[11] Moreover, the interparticle optical coupling varies significantly with nanometer-scale changes in gap distance[12] and orientation.[13] The ideal particle for self-assembly of plasmonic structures is therefore not a polyhedron, but a spherical crystal without facets or grain boundaries. However, producing such particles is a materials challenge, since spherical crystals are not stable under any growth conditions. Here we show that a cyclic process of slow growth followed by slow chemical etching, which selectively removes edges and vertices, results in ultra-smooth, highly spherical monocrystalline gold particles. The etching process, which is functionally similar to (but chemically different from) that used to make monocrystalline silver nanospheres for surface-enhanced Raman spectroscopy,[14,15] effectively makes the surface tension isotropic, so that spheres are favored under quasi-static conditions. The resulting spherical crystals display uniform scattering spectra and consistent optical coupling at small separations, even showing Fano-like resonances[16] in small assemblies. The cyclic process we demonstrate could be extended to other metals and, because it is scalable up to particle sizes of 200 nm or more, might be used to create strongly scattering particles for sensors,[17,18] electromagnetic resonators,[7] and other optical devices.[19]

The challenge of synthesizing metallic nanoparticles with controlled morphology is intimately connected to how crystals grow. Unlike silica or polymer nanoparticles, metallic nanoparticles are crystalline, and tend to adopt distinct facets when grown in a bulk suspension. As first described by Gibbs[20] and Wulff,[21] facets form because they minimize the surface free energy, which is a function of the exposed crystal planes. The number of facets can be controlled by chemically inhibiting the growth of certain crystal surfaces. This method has been used to produce nanoparticles with a variety of different shapes, including tetrahedra,[1] octahedra,[2,8] cubes,[8] and higher-order polyhedra.[3] However, even pseudo-spherical particles[22] produced this way have small facets.

We are not aware of any growth method that results in smooth, spherical nanocrystals. Quasi-spherical gold nanoparticles grown near equilibrium tend to increase in polydispersity and ellipsoidal eccentricity with increasing average particle diameter.[23,24] Nevertheless, fundamental studies of plasmonic phenomena[6,25] have proceeded under the assumption that such particles are adequate substitutes for spheres. An alternative is heterogeneous growth on a spherical dielectric shell, which produces nanoshells[26] that are spherical but polycrystalline, and as a result have rough

surfaces and grain boundaries that can lead to additional losses in plasmonic applications. Nanoshells are also subject to dewetting[27] and thermal instabilities.[28]

Our solution to this quandary is to use both growth and etching, rather than simply adjusting the growth conditions, to make solid gold nanospheres (Figure 1a). The growth step produces single-crystalline polyhedral particles, while the chemical etching step selectively removes edges and vertices while leaving the crystal structure intact. It is important that both steps are quasi-static, to avoid instabilities. The effect of the reduction-oxidation etching process is analogous to introducing an isotropic surface tension, which leads to spherical particles as the particle size decreases. By alternating between anisotropic growth and isotropic etching, we create smooth, spherical, single-crystalline particles of any desired size, up to 200 nm and conceivably larger. These spherical gold crystals are smoother than state-of-the-art polycrystalline or commercial particles and, as a result, show much more uniform optical properties, making them ideal building blocks for self-assembly of plasmonic nanostructures.
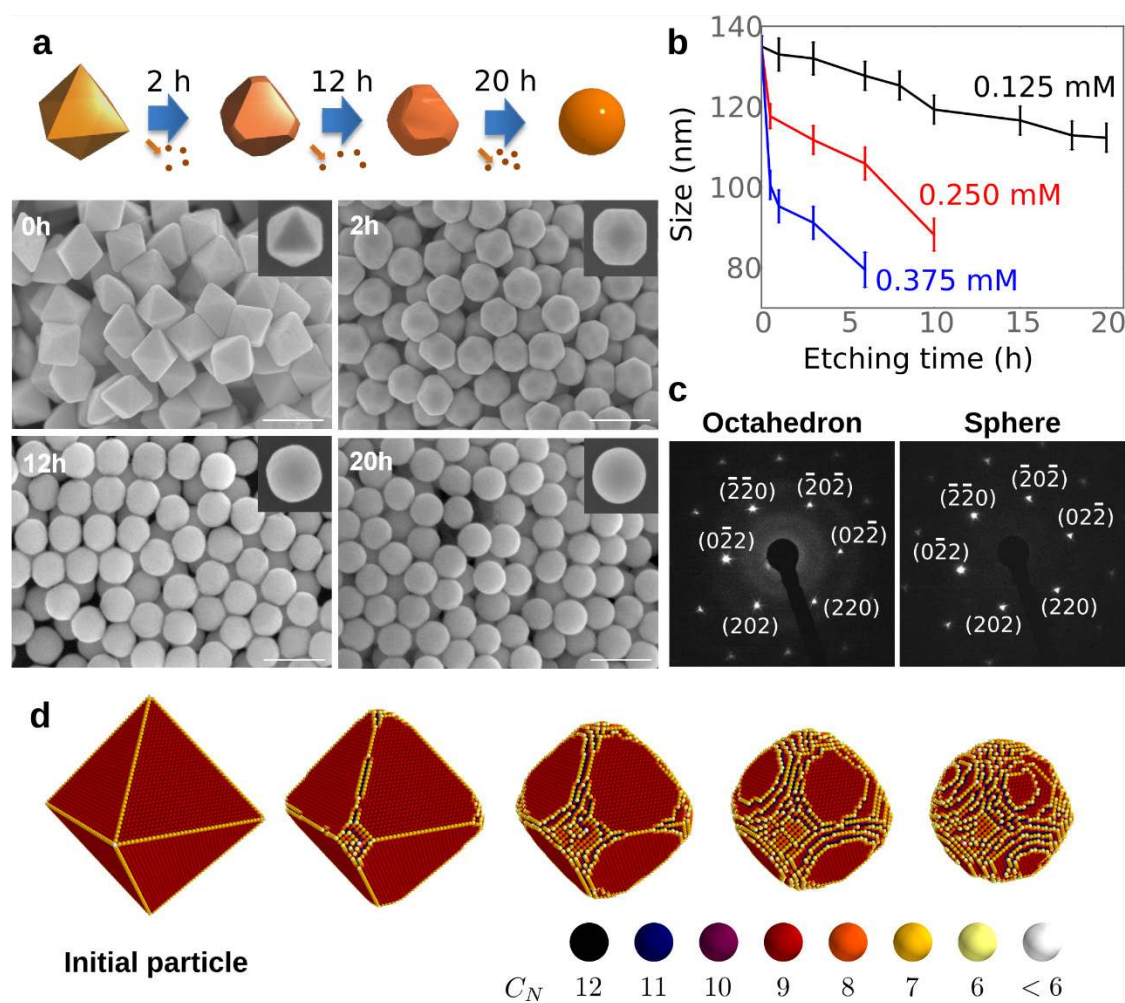
Figure 1. Growth followed by etching produces uniform, monocrystalline nanospheres. (a), Schematic diagram of shape evolution of gold particles during the etching process. SEM images of gold nanoparticles after chemical etching for various durations show the gradual transformation from octahedra to spheres. Scale bars are 200 nm. (b) Particle size as a function of etching time after the addition of $HAuCl_4$ in different concentrations. (c) Electron diffraction pattern of an octahedral particle and a spherical particle, showing that both are single crystals. (d) Sequential states in the simulated etching of a gold octahedron with edge length 40 atoms. The color of each atom corresponds to its coordination number and energy.

RESULTS AND DISCUSSION

Synthesis of uniform, monocrystalline gold nanospheres.
We start by synthesizing single-crystalline gold octahedra, following a procedure similar to that of Li *et al.*[2] (See Materials and Methods and Supporting Information for details.) The particles grow by the slow reduction of chloroauric acid ($HAuCl_4$) in ethylene glycol, which acts as a reducing agent at elevated temperature, with poly(diallyl dimethyl ammonium chloride) (polyDADMAC) and phosphoric acid (H_3PO_4). PolyDADMAC, a cationic polyelectrolyte, stabilizes the nanoparticles, and phosphoric acid controls the reduction rate of chloroauric acid.[2] The resulting uniform gold octahedra are 135.4 ± 12.5 nm in edge length (Figure 1a). A small number of particles with different shapes, such as decahedra and truncated triangular bipyramids, are also formed in this reaction but constitute less than 5% of the total.

To smooth the vertices and edges, we add an oxidizing agent, chloroauric acid, to the unwashed gold octahedron suspension after it cools. Chloroauric acid favors oxidation of the gold atoms specifically at vertices and edges, where the atoms have the lowest coordination.[29] Although chemical etching processes have been used to change the shape of polyhedral metal nanoparticles into exotic shapes, in general these processes do not produce uniform spheres.[30] Our etching process differs in that it is designed to be slow, so as to avoid instabilities leading to anisotropy, polydispersity, or significant reductions in particle size. Over the course of 20 hours, the particles progress from octahedra to truncated octahedra, quasi-spheres, and finally smooth gold nanospheres of diameter 112.3 ± 8.2 nm (Figure 1a). As shown in Figure 1b, the particle size decreases abruptly at first and then decreases more slowly as the oxidation-reduction reaction approaches equilibrium, and the chemical potential difference vanishes. Electron diffraction patterns of individual octahedra and spheres (Figure 1c) indicate that each nanoparticle is a single, face-centered cubic crystal, both before and after the etching reaction.

Monte Carlo simulations of the etching process, using atom energies calculated as a function of coordination number using the embedded atom method,[31] show that the oxidation conditions alone can explain the transformation to a sphere. The embedded atom method calculations predict that gold vertex atoms have a free energy of 26 k_BT and edge atoms of 10 k_BT relative to the [111] faces. These conditions favor the removal of vertices and edges before faces, as shown in Figure 1d and in Supplementary Movie 1. Although these simulations do not model diffusive dynamics, they do show that energetics favor the transition to a spherical morphology before the surface layers on the faces of the original octahedron are completely removed. Because the difference in free energy between faces is only 3.9 k_BT, the anisotropy in the surface tension is small compared to the difference in free energy between edges and faces, or between vertices and faces. Thus the surface tension is effectively isotropic, and it favors the removal of regions of high curvature.
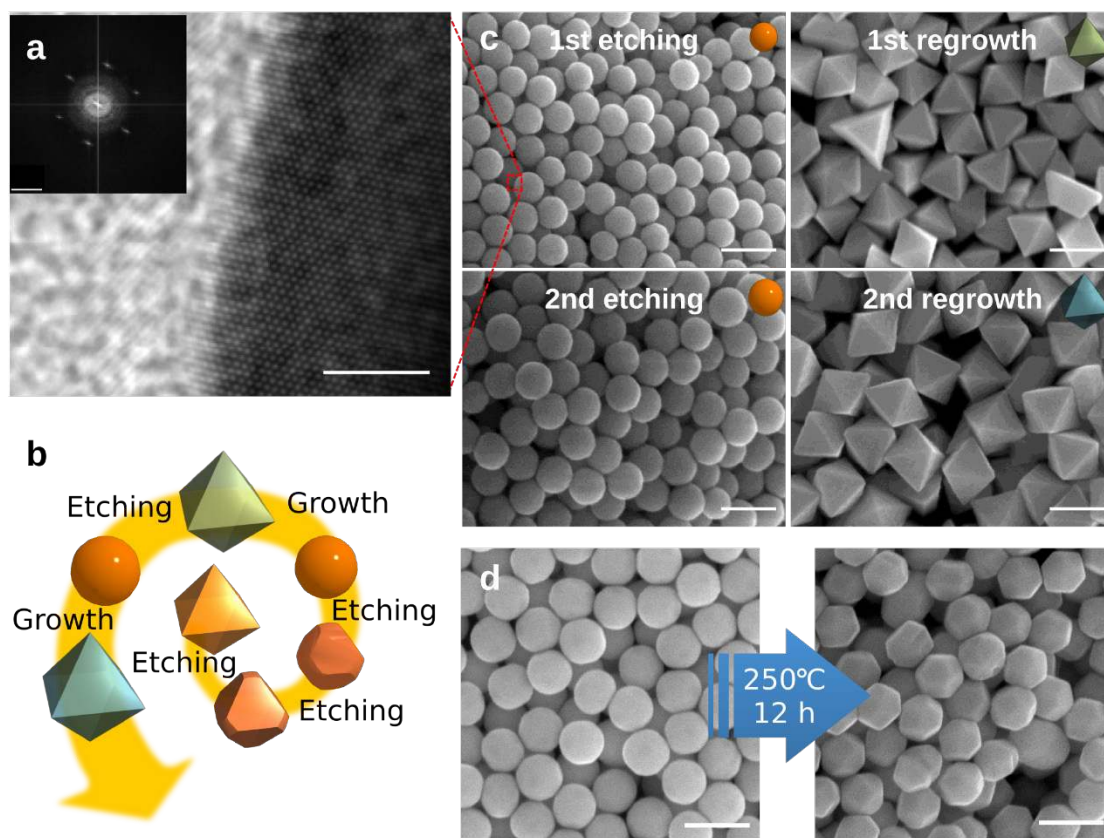
Figure 2. Nanospheres produced by growth and etching are single crystals that can be used as seeds for further growth. (a) High-resolution transmission electron micrograph of a gold nanosphere shows that the crystalline order extends to the edge of the particle. Scale bar is 2 nm. Inset shows the electron diffraction pattern. (b) Schematic diagram of iterated etching and regrowth of gold nanoparticles to produce large particles. (c) Scanning electron micrographs show particles after repeated etching and growth steps. Scale bars are 200 nm. (d) Scanning electron micrographs taken before and after annealing a sample of gold microspheres at 250 °C in pentanediol for 12 h. Scale bars are 200 nm.

Cyclic growth and etching process.

The etching process leaves the crystal structure of each particle unperturbed, resulting in true spherical crystals, as evidenced by high-resolution transmission electron micrographs (Figure 2a). To further confirm that the crystalline order extends to the boundary of the nanospheres, we used 112.3 ± 8.2 nm gold spheres produced by our growth and etching process as seeds for a second growth reaction (Figure 2b) (Materials and Methods). This resulted in larger octahedra with edge length 156.5 ± 13.8 nm (Figure 2c). If the original spheres were not monocrystalline, we would not expect that the regrowth reaction would result in such uniform and smooth octahedra.

The seeded growth experiments also illustrate a route to larger gold nanospheres through cyclic etching and growth. We initiated another etching reaction using the regrown octahedral particles and found that these too transformed into spheres. The new batch of nanospheres was larger (131.2 ± 9.5 nm) than the original seed spheres we had obtained after 20 hours. We produced larger octahedral gold particles in a third growth step (173.3 ± 15.1 nm), and as we continued this procedure, we obtained smooth gold spheres of diameter 200 nm after seven iterations (Supporting Information). We know of no other route to such large and uniform gold particles.

Annealing experiments (Supporting Information) show that these spherical crystals, though metastable with respect to the polyhedral morphology, are in fact more stable than quasi-spherical gold nanostructures. We find that in the absence of etching reagents, the nanospheres maintain their shape at temperatures up to 200 °C. At 250 °C, the particles start developing facets, as shown in Figure 2d. In contrast, gold nanoshells melt at temperatures as low as 175 °C due to grain boundaries and fissures.[28] The enhanced stability suggests that the spherical crystals are not only monocrystalline, but also have a low level of defects that might compromise thermal stability.
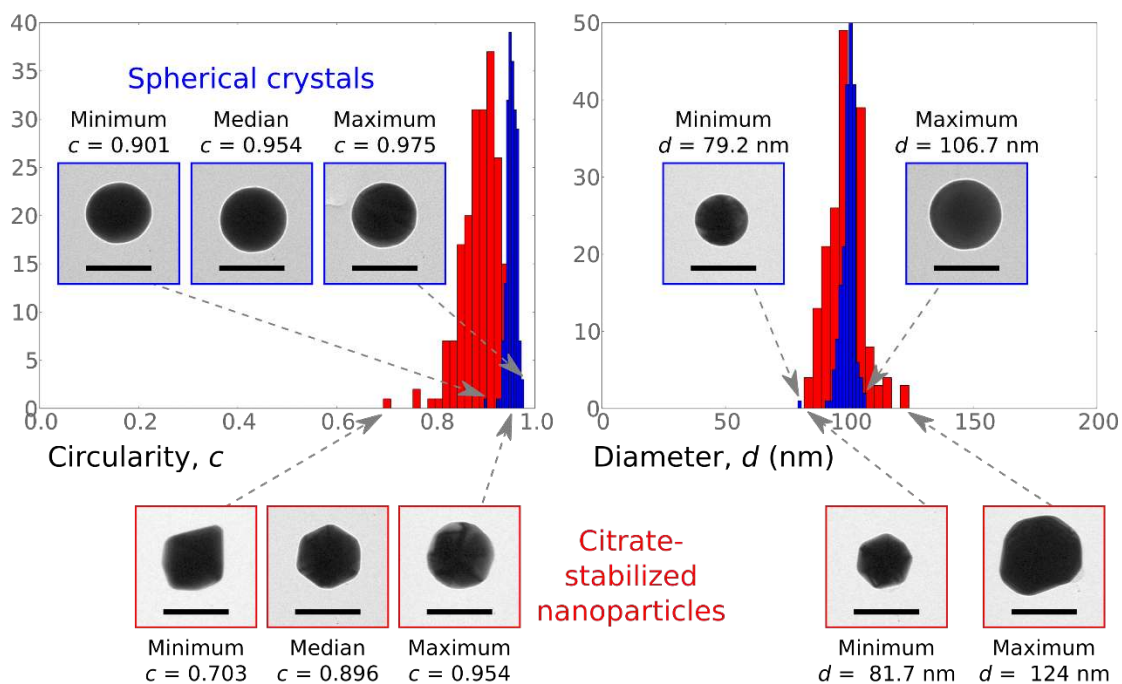
Figure 3. Distribution of circularity and diameter of spherical gold crystals (blue) and citrate-stabilized gold nanoparticles (red), as measured from TEM images of samples of 200 particles using image processing. A perfectly circular particle corresponds to $c = 1$; the circularity decreases toward zero as the particle's outline deviates from a circle. Insets show micrographs corresponding to key parts of each distribution. Scale bars are 100 nm.

Circularity and size distribution.

The other state-of-the-art particles for studies of plasmonic phenomena are quasi-spherical gold particles produced from citrate reduction of $HAuCl_4$ in water.[32,33] These have been used in several recent experiments to study phenomena such as surface enhanced Raman scattering,[18] Fano resonances,[6] nanoparticle-microcavity-based sensing,[34] and quantum limits of plasmonic coupling.[25] However, we find that these particles are much less smooth and spherical than the nanospheres produced through growth and etching. We quantify these differences using image analyses of transmission electron micrographs (Figure 3).

Starting with a TEM image of a single nanoparticle, we use the software program ImageJ to threshold and filter the image. We then sample over all angles in the plane of the image to compute the maximum Feret's diameter d_F of the region representing the nanoparticle. This represents the longest line segment that can be drawn from one side of the particle to another. We define the "circularity" c of the particle as the ratio of its area A in the filtered image to the area of a circle whose diameter is equal to d_F, expressed in the equation $c = 4A/\pi d_F^2$. A perfectly circular particle corresponds to $c = 1$; the circularity decreases toward zero as the particle's outline deviates from a circle. From the area A that we measure in each image, we can also compute an average diameter of each particle, $d = \sqrt{4A/\pi}$. From the distribution of d for each colloid, we can measure its polydispersity.

We measure c and d for equal numbers of gold nanospheres made through growth and etching and citrate-stabilized gold particles purchased from British Biocell International (BBI), which are prepared using a proprietary method based on the procedure developed by Turkevich, *et al.*[32] As shown in Figure 3, the distributions of the circularity, c, and the diameter, d, for these particles are more than twice as broad as they are for particles of comparable size from the growth and etching technique. The spherical crystals have an average diameter of 99.5 nm with a standard deviation of 2.9 nm. They are more monodisperse than a comparable sample of citrate-stabilized particles, whose average diameter is 98.8 nm with a standard deviation of 7.2 nm. Moreover, the median citrate-stabilized particle deviates from perfect circularity (1.000) more than twice as much as the median spherical crystal; the median circularity of the spherical crystals is 0.954 and that of the citrate-stabilized particles is 0.896.
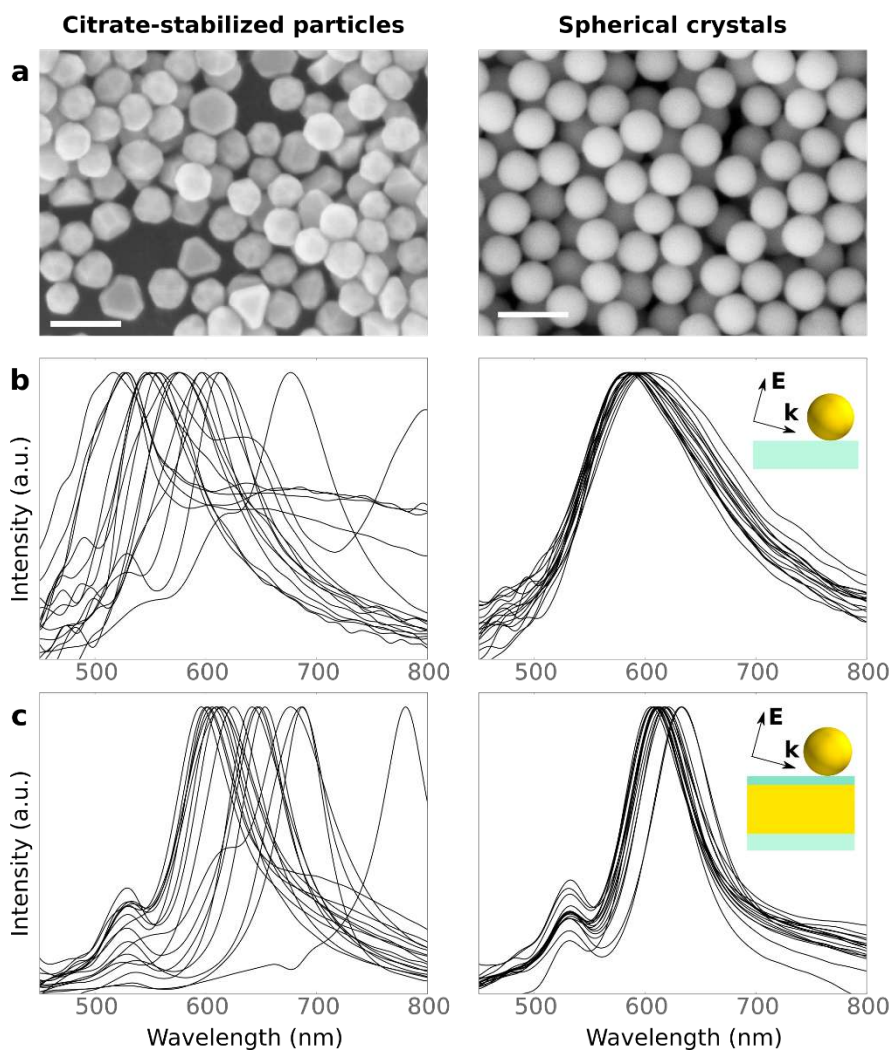
Figure 4. Reproducibility of gold nanoparticle scattering spectra. (a) Scanning electron micrographs of gold nanoparticles synthesized by citrate reduction or growth and etching. Scale bars are 200 nm. (b-c) measured scattering spectra for citrate-stabilized nanoparticles and spherical crystals. Particles in (b) are on a glass slide and in (c) a gold film with a thin dielectric spacer. Insets show polarization direction.

Reproducible scattering spectra of gold nanospheres.
The qualitative advances in particle uniformity, sphericity, smoothness, stability, and monocrystallinity afforded by the growth and etching technique (Figure 4a) enable the assembly of plasmonic structures with uniform and reproducible optical properties. We demonstrate this through several experiments examining the spectra of individual particles and assemblies thereof. To test the optical uniformity of the nanospheres, we record dark-field scattering spectra from individual particles deposited on a glass slide (Materials and Methods), shown in Figure 4b. We find that the standard deviation of the resonance peak wavelength for our spherical crystals is 5.7 nm, nearly 7 times smaller than that of commercial citrate-stabilized particles.

The nanospheres also show uniform spectra when their surface plasmons interact with those of a metal surface only 10 nm away. Unlike individual particles on a glass slide, this system enables us to probe higher-order plasmon modes in the context of coupling. We place the particles on a smooth gold film with an aluminum oxide spacer (Materials and Methods) and measure their scattering spectra with p-polarized light at a 65° angle of incidence. In this geometry, the interaction results in a low-energy bonding mode and a higher energy anti-bonding mode, both of which are broadened due to the finite film thickness.[35] We find that for the nanospheres produced through growth and etching, the standard deviation in peak wavelength is nearly 6 times smaller than it is for citrate-stabilized particles of similar size (Figure 4c). Furthermore, features like the smaller peak near 530 nm and the minimum near 550 nm are more reproducible for the spherical crystals than for the citrate-stabilized particles, some of which don't exhibit these features at all. For the spherical crystals, the wavelength of the small peak has a standard deviation of only 0.74 nm and may in fact be much smaller, as this value is comparable to the instrumental broadening of our spectrometer apparatus; for the citrate-stabilized particles the distribution is nearly 5 times as broad. The standard deviation of the ratio of the small peak intensity to the minimum intensity is 3.5 times larger for citrate-stabilized particles than for spherical crystals. Because the coupling that leads to these features depends sensitively on azimuthal symmetry and the distance between the particle and the gold film,[35] the results suggest that nanospheres produced by growth and etching are round and smooth down to the nanometer scale.
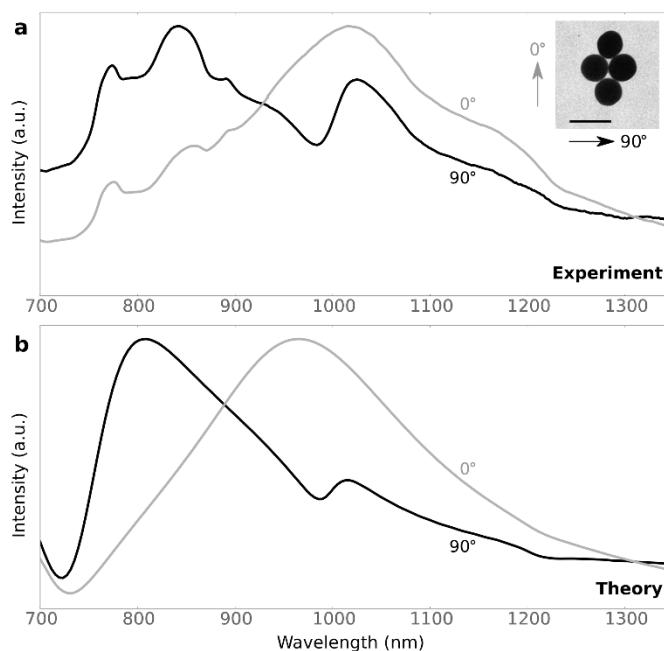
Figure 5. Scattering spectra of quadrumer cluster. (a) Experimental and (b) calculated near-normal incidence dark-field scattering spectra of a gold nanosphere quadrumer under long-axis (gray) and short-axis (black) polarization. Minima appear in both the experimental and calculated spectra near 980 nm when the polarization is parallel to the short axis of the quadrumer. We attribute this minimum to a Fano-like resonance because it occurs for only one polarization. Adsorption of organic molecules during the etching process results in a spacer on the order of 2 nm between the particles. Some discrepancies between the theoretical and experimental spectra at short wavelengths are likely due to scattering from other parts of the sample (SI) and have been observed in previous experiments.[5,16] Inset shows a transmission electron micrograph of a quadrumer. Scale bar is 200 nm.

Scattering spectra of quadrumer cluster.

To demonstrate that these particles may be used for self-assembly of artificial plasmonic molecules and other nanostructures showing complex coupling between plasmon modes, we prepare symmetric four-particle clusters ("quadrumers") on TEM grids (Materials and Methods) and measure their scattering spectra using near-normal incidence dark-field spectroscopy.[36] A narrow minimum appears in the spectrum near 980 nm when the polarization of the incident light is parallel to the quadrumer's short axis (Figure 5a). The minimum disappears when the polarization is parallel to the quadrumer's long axis. These spectral features, characteristic of a Fano-like resonance,[16] are in good agreement with calculated scattering spectra (Materials and Methods and SI, Figure 5b) for a quadrumer modeled by uniform, spherical gold nanoparticles. The resonance results from interference between quadrupolar and higher order modes of the nanoparticles.[16] This shows that the spherical nanocrystals can be used to fabricate plasmonic structures with similar properties to those made using gold nanoshells.[5]

CONCLUSION

The method we have demonstrated to produce highly uniform, single-crystalline gold nanospheres can be used to address longstanding problems in the field of plasmonics. Particles on the order of 100 nm and larger are important for many applications because the scattering cross section exceeds the absorbance cross section for gold particles larger than 80 nm.[17] The cyclic process we demonstrate can easily produce particles of 200 nm or larger, without the eccentricities and polydispersity typical of gold particles larger than 30 nm produced from established protocols. Indeed, conventional synthesis routes yield particles that are so heterogeneous that some groups have made use of the heterogeneity to fabricate asymmetric structures from a single batch of particles.[6] Furthermore, the high monodispersity of the particles we demonstrate should facilitate the self-assembly of nanoparticle clusters with uniform linear or non-linear optical resonances, which could in turn be used to fabricate optical metafluids[7] or to investigate enhanced optical four-wave mixing.[37] Narrow size distributions are required not only to control the spectral features, but also the morphology and yield of clusters in certain assembly schemes.[38] A similar cyclic process of anisotropic growth followed by isotropic etching could be used to design spherical crystals of other metals, which might find uses as building blocks for optical sensors and circuits,[18,19] probes for biomedical applications,[17,39] nucleation sites for nanobubble generation,[40,41] and components for other applications in which smoothness, thermal stability, and uniformity of the optical response are critical.

MATERIALS AND METHODS

Chemicals. Ethylene glycol (anhydrous, 99.8%), gold(III) chloride trihydrate (≥ 49.0% metals basis), poly(dimethyldiallylammonium chloride) (M_w 400,000 - 500,000, 20 wt % in H_2O), phosphoric acid (85 wt % in H_2O), chloroplatinic acid hydrate (99.995% metals basis), ethanol (a 99:5%), hexadecyltrimethylammonium bromide (≥ 99:0%), sodium dodecyl sulfate (92.5-100.5%), polyvinylpyrrolidone (M_w ~ 55,000) were purchased from Aldrich and used without further purification.

Synthesis of octahedral gold particles. A 20 mL anhydrous ethylene glycol solution was stirred with a magnetic bar in a glass vial and then 0.4 mL of polyDADMAC (20 wt % in H_2O, M_w 400,000 - 500,000) and 0.8 mL of 1 M H_3PO_4 solution were added. The mixture was stirred for 2 more minutes and 0.02 mL of a 0.5 M $HAuCl_4$ aqueous solution were added under stirring. The mixture was maintained at room temperature for 15 minutes, and then the solution in the glass vial was loaded into an oil bath for 30 minutes which was maintained at 195 °C throughout the reaction. During the reaction, the color of the solution changed from yellow to colorless and then, gradually, to purple and finally brown. We centrifuged the solution at 13,000 rpm and re-dispersed the precipitates in ethanol three times to remove the excess reactants and byproducts.

Chemical etching process of octahedral gold particles. To convert the octahedral gold nanoparticles to gold nanospheres, 5 μL of 0.5 M $HAuCl_4$ solution were added into the unwashed gold octahedra suspension (20 mL, 8.9×10^{-3} wt%) at room temperature. The color of the suspension changed from brown to pink. The size of the gold nanocrystals decreased from 135.4 ± 12.5 nm to 112.3 ± 8.2 nm over 20 h, and the gold nanocrystals evolved from octahedra to spheres.

Regrowth of spherical gold particles. The unwashed gold sphere suspension in a glass vial was loaded into an oil bath at 195 °C for 1 hour. We started with 112.3 ± 8.2 nm gold spheres in suspension with the 5 μL chloroauric acid that had previously been added for etching. After the first regrowth, we obtained octahedral particles of edge length 156 ± 13.8 nm (Figure 2c). Then, we etched the octahedral particles again by adding 5 μL of chloroauric acid; the resulting spheres (Figure 2d) were larger (131.2 ± 9.5 nm) than the original seed spheres we had obtained after 20 hours. During the reaction, the color of the suspension changed from orange-pink to brown as the particles evolved from spheres to octahedra.

Preparation of nanoparticles on a glass slide. We prepared samples for spectroscopy measurements by drying a droplet of dilute gold nanosphere suspension on a glass slide. The slide was treated with oxygen plasma at 60 W for 10 s to make the surface more hydrophilic. Immediately afterward we placed onto the slide a droplet of gold nanosphere suspension that had been sonicated for at least one minute

in a bath sonicator. We measured spectra from individual particles after the droplet dried in air. Both the spherical crystals and the citrate-stabilized particles were deposited on the same glass slide for dark-field spectroscopy measurements. Scanning electron microscopy confirmed that the vast majority of particles on the sample were well-dispersed, sitting several microns apart rather than occurring in clusters.

Preparation of particles on gold film separated by a dielectric layer. We prepared samples by drying a droplet of dilute gold nanosphere suspension on a substrate consisting of a thin Al_2O_3 layer on top of a template-stripped gold film supported on a glass slide. To prepare the substrate, we first deposited 120 nm of gold onto a cleaned silicon wafer with electron beam evaporation. Then we placed a small drop of UV curable epoxy (Norland Optical Adhesive 65 from Thorlabs, Inc.) on top of the gold film and put a glass slide on top before curing it under a UV lamp for 20 minutes. The wafer was stripped off of the film so that the film could be transferred entirely to the glass slide but retain a wafer-smooth surface. Next, 10 nm of Al_2O_3 were deposited onto the exposed surface of the gold film using atomic layer deposition (ALD). We treated the Al_2O_3 surface with oxygen plasma at 60W for 10 s to make the surface more hydrophilic and then immediately placed a droplet of gold nanosphere suspension on it. We let the droplet air-dry and then measured the spectra.

Self-assembly of plasmonic clusters and dark-field spectroscopy. Gold nanoparticle quadrumers were prepared by drying a droplet of dilute gold nanosphere suspension on a London finder Formvar TEM grid (LF200), purchased from Ted Pella. We placed 2 µL droplets of gold nanosphere colloid on the grids and let them air-dry. Some of the particles self-assembled into clusters on the Formvar surface due to capillary forces while drying.[5] Individual clusters were located on the grid using a Zeiss Libra 120 TEM operating at 60 keV, and micrographs were recorded at different magnifications so that the clusters could later be located (using the London finder grid pattern) with dark-field spectroscopy.[5] We conducted near-normal incidence dark-field spectroscopy as described in an earlier report.[36]

Numerical simulation of scattering spectra of gold nanosphere quadrumer. To calculate the quadrumer's scattering spectra we conducted finite-difference time-domain (FDTD) simulations at two different polarizations using the commercial software package Lumerical. The simulation assumed perfect spheres of diameter 130 nm with the optical properties of gold, following the Johnson and Christy standard.[42] The particle size in our model corresponded approximately to the size of the nanospheres in the quadrumer cluster whose scattering spectrum we measured. Additional FDTD simulation details are in the Supporting Information.

Supplementary Information Available: Supplemental Figures, Discussion, and Movie. This material is available free of charge *via* the Internet at http://pubs.acs.org.

REFERENCES AND NOTES

1. Zhou, J.; An, J.; Tang, B.; Xu, S.; Cao, Y.; Zhao, B.; Xu, W.; Chang, J.; Lombardi, J. R. Growth of Tetrahedral Silver Nanocrystals in Aqueous Solution and Their SERS Enhancement. *Langmuir* **2009**, *24*, 10407–10413.

2. Li, C.; Shuford, K. L.; Chen, M.; Lee, E. J.; Cho, S. O. A Facile Polyol Route to Uniform Gold Octahedra with Tailorable Size and Their Optical Properties. *ACS Nano* **2008**, *2*, 1760–1769.

3. Langille, M. R.; Zhang, J.; Personick, M. L.; Li, S.; Mirkin, C. A. Stepwise Evolution of Spherical Seeds into 20-Fold Twinned Icosahedra. *Science* **2012**, *337*, 954–957.

4. Tan, S. J.; Campolongo, M. J.; Luo, D.; Cheng, W. Building Plasmonic Nanostructures with DNA. *Nat. Nanotechnol.* **2011**, *6*, 268–276.

5. Fan, J. A.; Wu, C.; Bao, K.; Bao, J.; Bardhan, R.; Halas, N. J.; Manohanran, V. N.; Nordlander, P.; Shvets, G.; Capasso, F. Self-Assembled Plasmonic Nanoparticle Clusters. *Science* **2010**, *328*, 1135–1138.

6. Shafiei, F.; Monticone, F.; Le, K. Q.; Liu, X.-X.; Hartsfield, T.; Alù, A.; Li, X. A Subwavelength Plasmonic Metamolecule Exhibiting Magnetic-Based Optical Fano Resonance. *Nat. Nanotechnol.* **2013**, *8*, 95–99.

7. Urzhumov, Y. A.; Shvets, G.; Fan, J.; Capasso, F.; Brandl, D.; Nordlander, P. Plasmonic Nanoclusters: A Path Towards Negative-Index Metafluids. *Opt. Express* **2007**, *15*, 14129-14145.

8. Wang, Y.; Wan, D.; Xie, S.; Xia, X.; Huang, C. Z.; Xia, Y. Synthesis of Silver Octahedra with Controlled Sizes and Optical Properties *via* Seed-Mediated Growth. *ACS Nano* **2013**, *7*, 4586–4594.

9. Noguez, C. Surface Plasmons on Metal Nanoparticles: The Influence of Shape and Physical Environment. *J. Phys. Chem. C* **2007**, *111*, 3806–3819.

10. Lin, H.-X.; Li, J.-M.; Liu., B.-J.; Liu, D.-Y.; Liu, J.; Terfort, A.; Xie, Z.-X.; Tian, Z.-Q.; Ren, B. Uniform Gold Spherical Particles for Single-Particle Surface-Enhanced Raman Spectroscopy. *Phys. Chem. Chem. Phys.* **2013**, 15, 4130–4135.

11. Liz-Marzán, L. M. Tailoring Surface Plasmons through the Morphology and Assembly of Metal Nanoparticles. *Langmuir* **2006**, *22*, 32–41.

12. Lassiter, J. B.; Aizpurua, J.; Hernandez, L. I.; Brandl, D. W.; Romero, I.; Lal, S.; Hafner, J. H.; Nordlander, P.; Halas, N. J. Close Encounters Between Two Nanoshells. *Nano Lett.* **2008**, *8*, 1212–1218.

13. Henzie, J.; Andrews, S. C.; Ling, X. Y.; Li, Z.; Yang, P. Oriented Assembly of Polyhedral Plasmonic Nanoparticle Clusters. *Proc. Natl. Acad. Sci. U. S. A.* **2013**, *110*, 6640–6645.

14. Cobley, C. M.; Rycenga, M.; Zhou, F.; Li, Z.-Y.; Xia, Y. Controlled Etching As a Route to High Quality Silver Nanospheres for Optical Studies. *J. Phys. Chem. C.* **2009** *113*, 16975-16982.

15. Xiong, Y. Morphological Changes in Ag Nanocrystals Triggered by Citrate Photoreduction and Governed by Oxidative Etching. *Chem. Commun. (Cambridge, U. K.)* **2011**, *47*, 1580-1582.

16. Fan, J. A.; Bao, K.; Wu, C.; Bao, J.; Bardhan, R.; Halas, N. J.; Manoharan, V. N.; Shvets, G.; Nordlander, P.; Capasoo, F. Fano-Like Interference in Self-Assembled Plasmonic Quadrumer Clusters. *Nano Lett.* **2010**, *10*, 4680–4685.

17. Anker, J. N.; Hall, W. P.; Lyandres, O.; Shah, N. C.; Zhao, J.; Van Duyne, R. P. Biosensing with Plasmonic Nanosensors. *Nat. Mater.* **2008**, *7*, 442–453.

18. Lim, D.-K.; Jeon, K.-S.; Hwang, J.-H.; Kim, H.; Kwon, S.; Suh, Y. D.; Nam, J.-

M. Highly Uniform and Reproducible Surface-Enhanced Raman Scattering from DNA-Tailorable Nanoparticles with 1-nm Interior Gap. *Nat. Nanotechnol.* **2011**, *6*, 452–460.

19. Engheta, N. Circuits with Light at Nanoscales: Optical Nanocircuits Inspired by Metamaterials. *Science* **2007**, 317, 1698–1702.

20. Gibbs, J. W. On the Equilibrium of Heterogeneous Substances. In *The Collected Works of J. Willard Gibbs*; Bumstead, H. A., Longley, W. R., Eds.; Vol. 1; Longmans, Green and Company: New York, 1928; pp 314-331.

21. Wulff, G. Zur Frage der Geschwindigkeit des Wachstums und der Auflösung der Kristallflächen. *Z. kristallogr.* **1901**, *34*, 449–530.

22. Li, C. R.; Lu, N. P.; Mei, J.; Dong, W. J.; Zheng, Y. Y.; Gao, L.; Tsukamoto, K.; Cao, Z. X. Polyhedral to Nearly Spherical Morphology Transformation of Silver Microcrystals Grown from Vapor Phase. *J. Cryst. Growth* **2011**, *314*, 324–330.

23. Goodman, S. L.; Hodges, G. M.; Trejdosiewicz, L. K.; Livingston, D. C. Colloidal Gold Markers and Probes for Routine Application in Microscopy. *J. Microsc. (Oxford, U. K.)* **1981**, *123*, 201-213.

24. Grabar, K. C.; Brown, K. R.; Keating, C. D.; Stranick, S. J.; Tang, S.-L.; Natan, M.-J. Nanoscale Characterization of Gold Colloid Monolayers: A Comparison of Four Techniques. *Anal. Chem.* **1997**, *69*, 471–477.

25. Ciracì, C.; Hill, R. T.; Mock, J. J.; Urzhumov, Y.; Fernández-Domínguez, A. I.; Maier, S. A.; Pendry, J. B.; Chilkoti, A.; Smith, D. R. Probing the Ultimate Limits of Plasmonic Enhancement. *Science* **2012**, *337,* 1072–1074.

26. Oldenburg, S. J.; Averitt, R. D.; Westcott, S. L.; Halas, N. J. Nanoengineering of Optical Resonances. *Chem. Phys. Lett.* **1998**, 288, 243–247.

27. Tesler, A. B.; Chuntonov, L.; Karakouz, T.; Bendikov, T. A.; Haran, G.; Vaskevich, A.; Rubinstein, I. Tunable Localized Plasmon Transducers Prepared by Thermal Dewetting of Percolated Evaporated Gold Films. *J. Phys. Chem. C* **2011**, *115*, 24642–24652.

28. Radloff, C.; Halas, N. J. Enhanced Thermal Stability of Silica-Encapsulated Metal Nanoshells. *Appl. Phys. Lett.* **2001**, *79*, 674–676.

29. Hong, S.; Shuford, K. L.; Park, S. Shape Transformation of Gold Nanoplates and Their Surface Plasmon Characterization: Triangular to Hexagonal Nanoplates. *Chem. Mater.* **2011**, *23*, 2011–2013.

30. Xia, Y.; Xiong, Y.; Lim, B.; Skrabalak, S. E. Shape-Controlled Synthesis of Metal Nanocrystals: Simple Chemistry Meets Complex Physics? *Angew. Chem., Int. Ed.* **2009**, *48*, 60-103.

31. Foiles, S. M.; Baskes, M. I.; Daw, M. S. Embedded-Atom-Method Functions for the FCC Metals Cu, Ag, Au, Ni, Pd, Pt, and Their Alloys. *Phys. Rev. B* **1986**, *33*, 7983–7991.

32. Turkevich, J.; Stevenson, P. C.; Hillier, J. A Study of the Nucleation and Growth Processes in the Synthesis of Colloidal Gold. *Discuss. Faraday Soc.* **1951**, *11*, 55–75.

33. Frens, G. Controlled Nucleation for the Regulation of the Particle Size in Monodisperse Gold Suspensions. *Nature (London), Phys. Sci.* **1973**, *241*, 20–22.

34. Schmidt, M. A.; Lei, D. Y.; Wondraczek, L.; Nazabal, V.; Maier, S. A. Hybrid Nanoparticle-Microcavity-Based Plasmonic Nanosensors with Improved Detection Resolution and Extended Remote-Sensing Ability. *Nat. Commun.* **2012**, *3*, 1108.

35. Le, F.; Lwin, N. Z.; Steele, J. M.; Käll, M.; Halas, N. J.; Nordlander, P. Plasmons in the Metallic Nanoparticle–Film System As a Tunable Impurity

Problem. *Nano Lett.* **2005**, *5*, 2009–2013.

36. Fan, J. A.; Bao, K.; Lassiter, J. B.; Bao, J.; Halas, N. J.; Nordlander, P.; Capasso, F. Near-Normal Incidence Dark-Field Microscopy: Applications to Nanoplasmonic Spectroscopy. *Nano Lett.* **2012**, *12*, 2817–2821.

37. Zhang, Y.; Wen, F.; Zhen, Y.-R.; Nordlander, P.; Halas, N. J. Coherent Fano Resonances in a Plasmonic Nanocluster Enhance Optical Four-Wave Mixing. *Proc. Natl. Acad. Sci. U. S. A.* **2013**, *110*, 9215-9219.

38. Schade, N. B.; Holmes-Cerfon, M. C.; Chen, E. R.; Aronzon, D.; Collins, J. W.; Fan, J. A.; Capasso, F.; Manoharan, V. N. Tetrahedral Colloidal Clusters from Random Parking of Bidisperse Spheres. *Phys. Rev. Lett.* **2013**, *110*, 148303.

39. Peng, G.; Tisch, U.; Adams, O.; Hakim, M.; Shehada, N.; Broza, Y. Y.; Billan, S.; Abdah-Bortnyak, R.; Kuten, A.; Haick, H. Diagnosing Lung Cancer in Exhaled Breath Using Gold Nanoparticles. *Nat. Nanotechnol.* **2009**, *4*, 669–673.

40. Neumann, O.; Urban, A. S.; Day, J.; Lal, S.; Nordlander, P.; Halas, N. J. Solar Vapor Generation Enabled by Nanoparticles. *ACS Nano* **2013**, *7*, 42-49.

41. Fang, Z.; Zhen, Y.-R.; Neumann, O.; Polman, A.; de Abajo, F. J. G.; Nordlander, P.; Halas, N. J. Evolution of Light-Induced Vapor Generation at a Liquid-Immersed Metallic Nanoparticle. *Nano Lett.* **2013**, *13*, 1736-1742.

42. Johnson, P. B.; Christy, R. W. Optical Constants of the Noble Metals. *Phys. Rev. B* **1972**, *6*, 4370–4379.

SUPPORTING INFORMATION FOR
"Ultrasmooth, Highly Spherical Monocrystalline Gold Particles for Precision Plasmonics"

You-Jin Lee,[†, ‡ ,+] Nicholas B. Schade,[§,+] Li Sun,[⊥,+] Jonathan A. Fan,[#] Doo Ri Bae,[‡] Marcelo M. Mariscal,[¶] Gaehang Lee,[‡,*] Federico Capasso,[⊥] Stefano Sacanna,[∥] Vinothan N. Manoharan,[⊥,§] Gi-Ra Yi[†,*]

1. Synthesis of octahedral gold nanoparticles

Octahedral particles were synthesized by a modified polyol process as described in a previous report by Li, *et al.*[1] When we used hydrochloric acid, we always found octahedral particles smaller than 100 nm, and we also found many byproducts from the reaction, including dodecahedra and trigonal plates. We tested several different acids and we found that phosphoric acid produced larger octahedral particles (> 100 nm) with the fewest impurities. The exact reason for the better results with phosphoric acid is not clearly understood.

2. Etching octahedral particles to form spheres

At room temperature, ethylene glycol no longer behaves as a reducing agent, so growth of the nanocrystals is suppressed and the addition of chloroauric acid initiates an etching reaction. This etching process is driven by redox reactions and the concentration of $HAuCl_4$ controls the etching rate. To investigate this, we added three different amounts of chloroauric acid to equal volumes of unwashed octahedral particles. As shown in Figure 1b of our manuscript, decreasing the concentration of chloroauric acid slows the etching rate over the 20 h period.

To investigate whether there was another adjuvant that played a critical role in etching the gold octahedral particles, we tested the chemical ingredients used in our experiments. Only the mixture of $HAuCl_4$, polyDADMAC, and gold octahedral particles suspended in ethylene glycol exhibited a color change to orange (Figure S1a), accompanied by the transformation of the octahedra into spheres (Figure S1b-g). PolyDADMAC may form a complex with $AuCl_2^-$ when Au from the octahedral particles is oxidized. Consequently, the removal of gold atoms from the octahedra continues as the product of this reversible reaction is steadily removed. It is well known that complexation of $AuCl_4^-$ and $AuCl_2^-$ with a surfactant facilitates oxidation of Au^0, although the standard oxidation potentials of Au^0 to $AuCl_4^-$ and $AuCl_2^-$ are large negative values (respectively -1.002 and -1.154 V, versus a normal hydrogen electrode) and the equilibrium constant for reaction S1 is very low.[2]

$$AuCl_4^- + 2Au^0 + 2Cl^- \leftrightarrow 3AuCl_2^-, \ K = 1.9 \text{ X } 10^{-8} \qquad (S1)$$

This suggests that the etching rate may depend on the quantity of polyDADMAC added. In control experiments, we added only 1/10 or 1/100 of the normal amount of polyDADMAC solution to the gold octahedron suspension, waited 20 hours as usual, and observed larger, less smooth Au particles (Figure S2). This indicates that less etching occurs when less polyDADMAC is added. We tested other surfactants in addition to polyDADMAC and the results are shown in Figure S3. Cetyltrimethyl ammonium bromide (CTAB, a cationic surfactant) was effective in the chemical etching process but sodium dodecyl sulfate (SDS, an anionic surfactant) and polyvinylpyrrolidone (PVP, a nonionic surfactant) were not. CTAB may form complexes with gold chloride anions, however, as has already been reported in previous articles.[2,3] Moreover, because of the relatively high viscosity of ethylene glycol, the particles were stable against sedimentation and ions presumably diffused slowly, which made it possible to control the extent and uniformity of chemical etching.
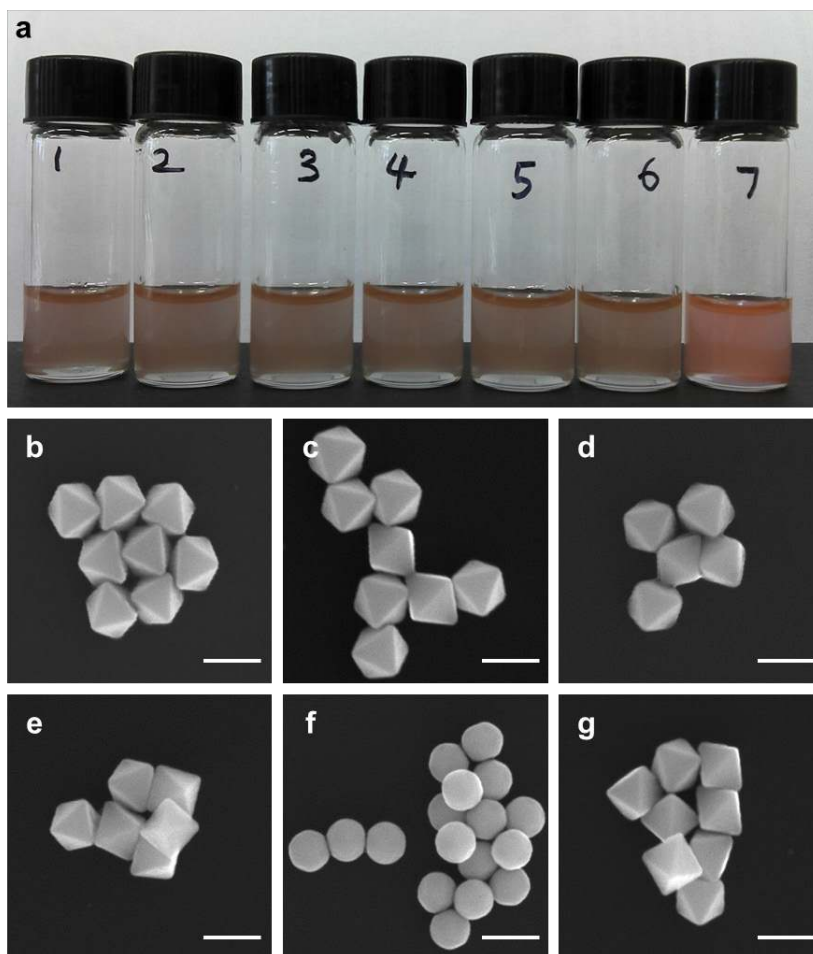
Figure S1. (a) Photographs of (1) the Au octahedron colloid solution before etching (20 mL, 8.9×10^{-3} wt%), and with the addition of (2) polyDADMAC (20 wt%, 0.4 mL); (3) H$_3$PO$_4$ (1 M, 0.8 mL); (4) HAuCl$_4$ (0.5 M, 5 µL); (5) polyDADMAC and H$_3$PO$_4$; (6) H$_3$PO$_4$ and HAuCl$_4$; or (7) polyDADMAC and HAuCl$_4$. SEM images of gold particles from a suspension (20 mL, 8.9×10^{-3} wt%) after adding (b) polyDADMAC aqueous solution (20 wt% in H$_2$O, 0.4 mL); (c) H$_3$PO$_4$ aqueous solution (1 M, 0.8 mL); (d) HAuCl$_4$ (0.5 M, 5 µL) aqueous solution; (e) poly-DADMAC and H$_3$PO$_4$; (f) H$_3$PO$_4$ and HAuCl$_4$; or (g) polyDADMAC and HAuCl$_4$. Scale bars are 200 nm.
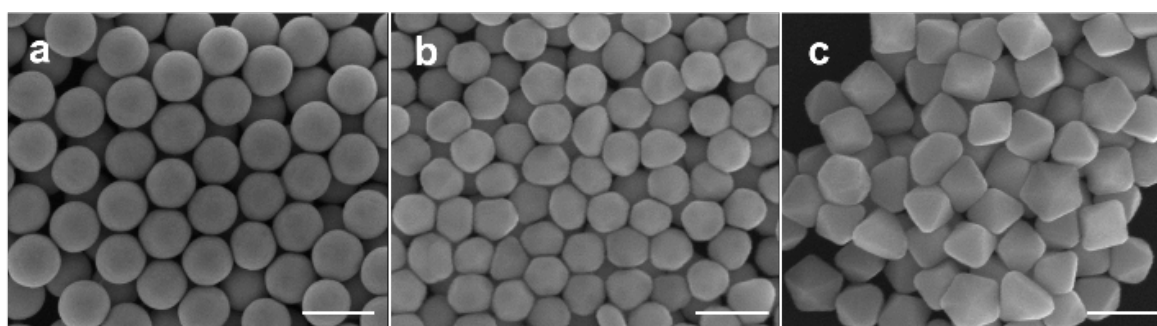

Figure S2. SEM images of Au particles after the addition of HAuCl$_4$ (0.5 M, 5 µL) and (a) 400 µL, (b) 40 µL, or (c) 4 µL of polyDADMAC into the washed gold suspension for a reaction time of 20 h. Scale bar: 200 nm.
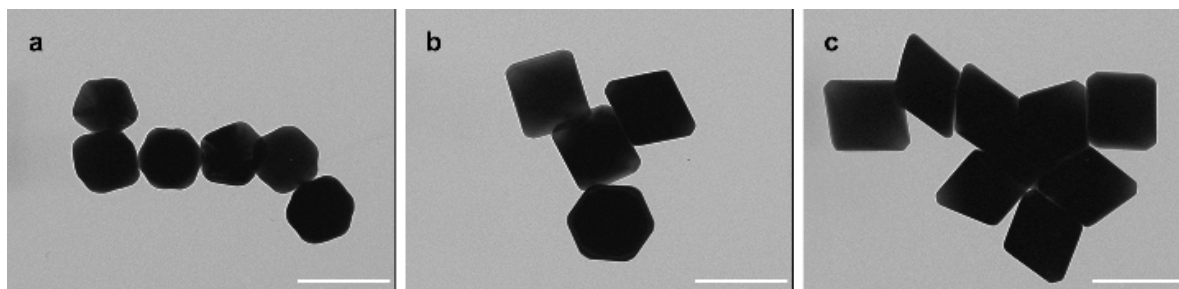
Figure S3. TEM images of Au colloids after the addition of HAuCl$_4$ (0.5 M, 5 µL) and (a) CTAB (20 wt% in H$_2$O, 0.4 mL), (b) SDS (20 wt% in H$_2$O, 0.4 mL), or (c) PVP (20 wt% in H$_2$O, 0.4 mL) to the Au octahedron solution. Scale bar: 200 nm.

To investigate the etching rate's dependence on chloroauric acid, we tested three different amounts of chloroauric acid with the same quantity of polyDADMAC (0.4 mL), as discussed in the main text of our letter. We found that decreasing the concentration of gold salt slowed the etching rate over the 20 h period. We determined the particle sizes as functions of reaction time from measurements of SEM images of samples taken at different times during the experiment (Figure S4). In all cases, the particle size decreased abruptly at first and then saturated as the oxidation-reduction reaction approached equilibrium and the chemical potential difference vanished.
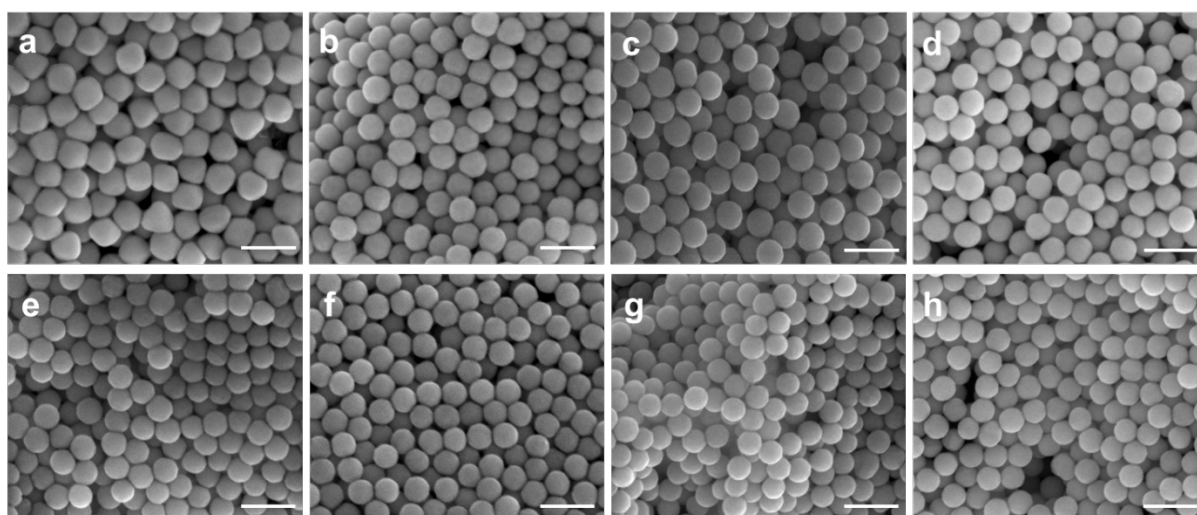

Figure S4. SEM images of the gold nanocrystals (a) 30 min., (b) 3 h, (c) 6 h, and (d) 10 h after the etching reaction began with 10 µL gold precursor. And SEM images of the gold nanocrystals (e) 30 min., (f) 1 h, (g) 3 h, and (h) 6 h after the etching reaction began with 15 µL gold precursor. Scale bars are 200 nm.

To understand how the different initial nanocrystal morphologies transformed during the etching reaction, we used SEM to observe samples of the mixture from various times throughout the etching process. The octahedral particles transformed into spheres through etching fastest (Figure S5). The truncated triangular bipyramids changed shape at a slower rate but they all eventually became spheres. The final gold spheres are uniform in size and shape regardless of the seed particles' shapes. X-ray diffraction (XRD) patterns in Figure S6 reveal that the {111} facet is dominant for the gold octahedron, in agreement with observations by other groups.[1,4] Other crystal planes including {200}, {220}, and {311}, consistent with the standard spectrum of fcc gold (JCPDS no. 89-3697), are also exposed at surfaces during the chemical etching process.
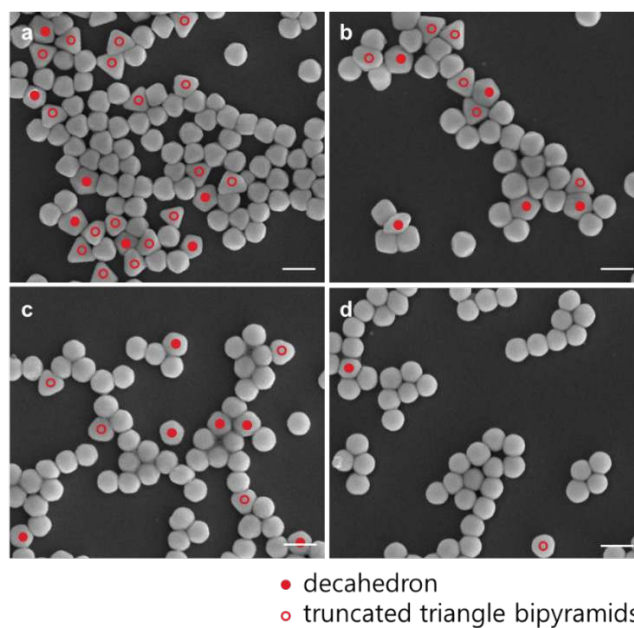
· decahedron
○ truncated triangle bipyramids

Figure S5. SEM images of the gold nanocrystals (a) 3 min., (b) 6 min., (c) 50 min., and (d) 4 h after the etching reaction began with 5 µL gold precursor. Scale bars are 200 nm.
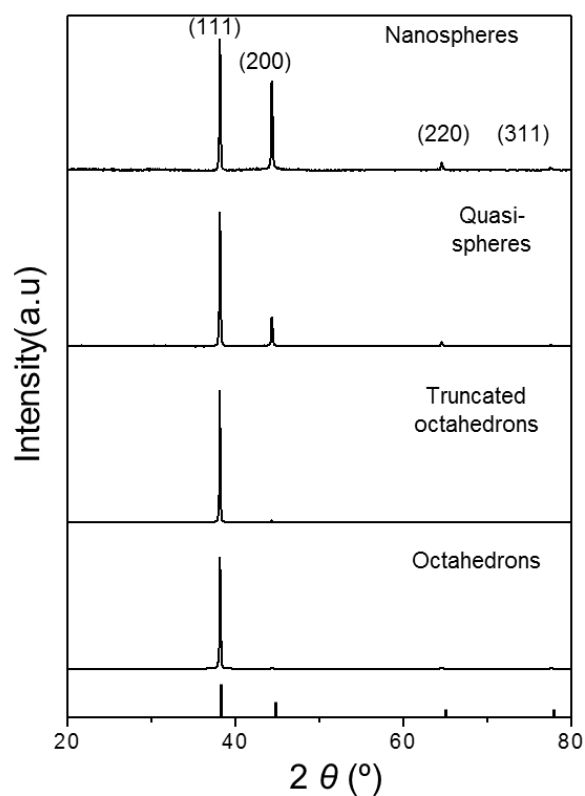

Figure S6. XRD patterns of gold structures from octahedron to truncated octahedron, quasi-sphere, and sphere. The standard XRD patterns for fcc gold (JCPDS no. 89-3697) are shown as a bar diagram at bottom.

3. Iterative growth and etching

In one experiment, we used our spherical gold crystals as seeds for octahedral re-growth. We initiated another etching reaction using these re-grown octahedral particles and found that these too transformed into spheres. We produced larger octahedral gold particles in a third growth step, and as we continued this procedure, we obtained larger smooth gold octahedra after each successive iteration. Electron micrographs of the resulting spheres and octahedra after successive iterations are shown in Figure S7.
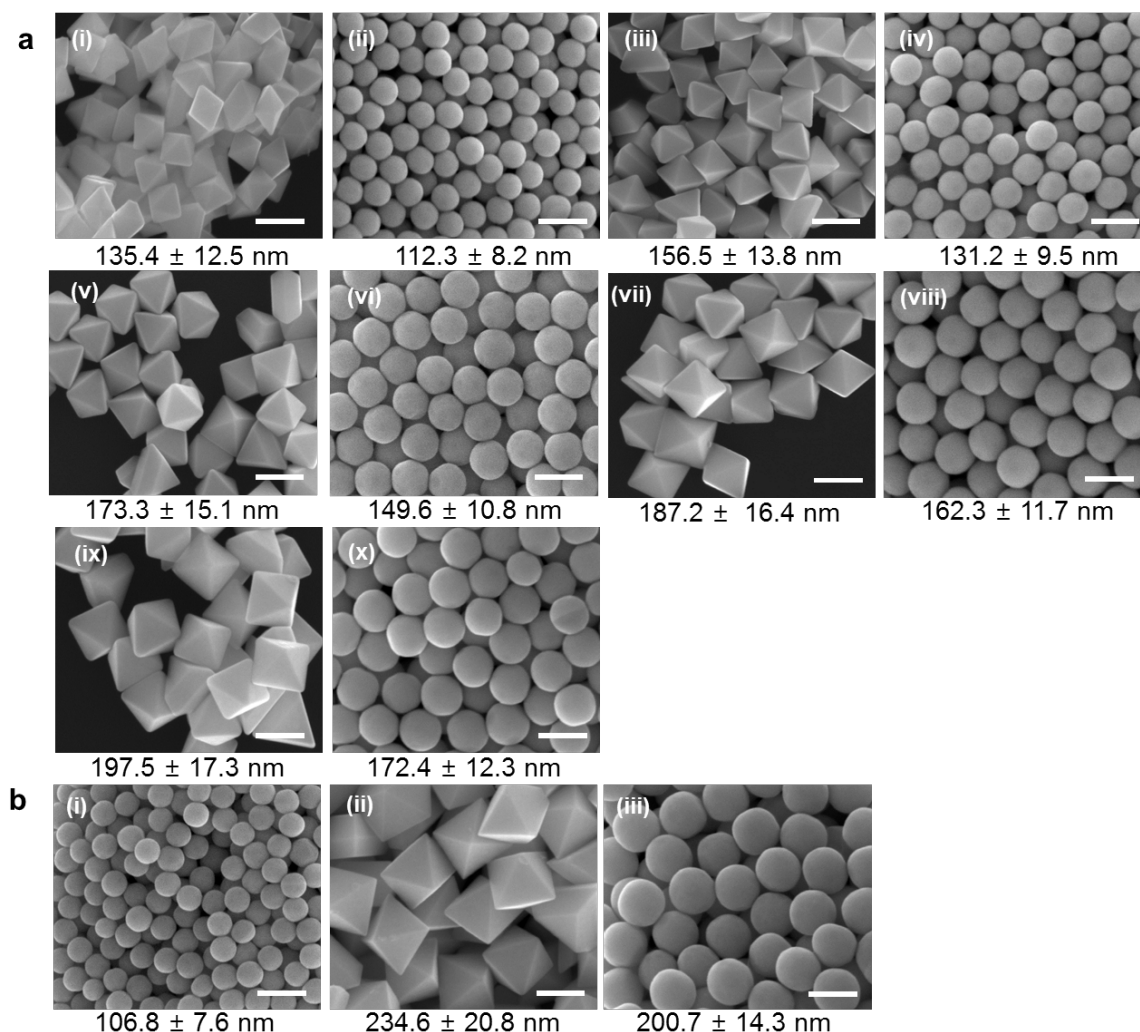

Figure S7. Iterative growth and etching of gold octahedra. a, (i-x) SEM images of gold octahedra and nanospheres after iterative growth and etching with addition of 5 μL aqueous HAuCl$_4$ solution. (i) initial growth, (ii) 1st etching, (iii) 1st regrowth, (iv) 2nd etching, (v) 2nd regrowth, (vi) 3rd etching, (vii) 3rd regrowth, (viii) 4th etching, (ix) 4th regrowth, (x) 5th etching. b, With the addition of 20 μL of 0.5 M aqueous HAuCl$_4$ solution, (i) smaller gold nanospheres and (ii) larger gold octahedra were produced from 197.5 nm gold octahedra shown in a(ix) and then (iii) 200.7 nm gold nanospheres were produced by etching 234.6 nm gold nanospheres in b(ii) with the addition of 5 μL of 0.5 M aqueous HAuCl$_4$ solution. Average particle sizes refer to edge length for octahedra and diameters for spheres. Scale bars are 200 nm.

4. Transformation back to polyhedra at high temperature

As discussed in the main text of our letter, we conducted an annealing experiment to test the stability of our gold nanospheres in the absence of the etching reaction. We washed a batch of spherical gold crystals more than 10 times in ethanol and redispersed them in 1,5-pentanediol. We then heated the mixture to just below the boiling point of pentanediol (250 °C) for half an hour. We found that under these conditions, the particles gradually transform back to polyhedra, as shown in Figure S8. Facets begin to form on the particles in less than 30 minutes. After 12 hours, the particles show significant faceting and some of them have merged together as dimers. Many of them appear to have adopted a truncated octahedral morphology, in agreement with predicted shape transformations prior to melting.[5] This implies that increased mobility at the crystal surface at 250 °C is sufficient to transform the particles to a faceted morphology. In a similar experiment, we washed and redispersed gold nanospheres in ethylene glycol and heated the suspension nearly to its boiling point (200 °C) for 12 hours. These particles showed no evidence of morphological transformation.
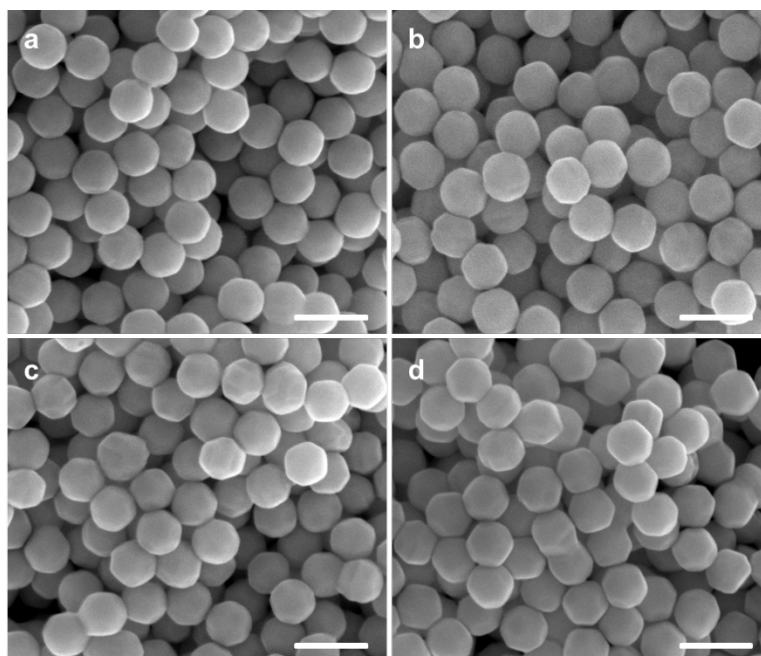

Figure S8. SEM images of Au particles after the solvo-thermal process in 1,5-pentanediol at 250 °C for a total reaction time of (a) 5 min, (b) 10 min, (c) 15 min, and (d) 30 min. Scale bars are 200 nm.

5. Numerical simulation of chemical etching

Starting with an octahedral nanoparticle defined in a space of fcc lattice sites, we calculate the energy of each atom based on its coordination number using the embedded atom method.[7] We then proceed with a grand canonical Metropolis algorithm[8-10] to select lattice sites at the surface of the crystal for either the insertion or removal of one atom at a time. The probability of insertion is determined from the change in free energy that would result,

$$W_{n \rightarrow n+1} = min\left(1, \frac{V_{acc}}{X\Lambda^3(n+1)}e^{\left(\mu - \frac{\Delta E_{n+1,n}}{k_B T}\right)}\right) \qquad (S2)$$

similar to the method explained in a previous study,[10] with a few differences. In equation S2, n is the number of atoms in the nanocrystal and Λ is the thermal wavelength, given by $\left(\frac{h}{2\pi m k_B T}\right)$. The volume where particles can be created V_{acc} is given by the number of occupied and unoccupied lattice sites with coordination number CN > 0 multiplied by the volume of a gold atom, $\left(\frac{4}{3}\pi r_{Au}^3\right)$. Thus it includes not only the volume of the crystal itself but also the volume of a surface layer of lattice sites where an atom could be inserted such that it would form at least one bond with another atom already in the crystal. The chemical potential is calculated from $\mu = RT \ln a_M$, where the activity a_M is taken as the initial concentration of chloroauric acid added to start the reaction. Molecules in solution at and outside the surface of the nanocrystal are not modeled.

One difference between the present algorithm and the previous study[10] is that the change in energy due to the insertion of an atom, $\Delta E_{n+1,n}$, includes not only the decrease in energy from forming bonds with other atoms but also an energy increase of 3.700 eV due to the etching reaction. This value is the difference between the reduction potential (-0.228 eV) of reaction S1, calculated from reduction potentials for half-reactions reported elsewhere[3], and the binding energy of the atoms in the bulk of the crystal with $CN = 12$, which is -3.928 eV according to embedded atom method calculations.

Another difference in the present algorithm is that the probability is normalized by dividing by a large constant, X, chosen throughout the present study to be 10^9. This has the effect of slowing the entire simulation down, while introducing a preference for the insertion or removal of atoms at sites where the change results in a larger decrease in the system's free energy. We include this factor so that we can observe which areas of the crystal are modified first preferentially. This modification to the standard grand canonical Metropolis algorithm is acceptable because it should have no effect on the equilibrium state to which the simulation converges. We are not primarily interested in the equilibrium state anyway, which in this case is the dissolution of the crystal entirely. Instead, we are interested in how the system gradually changes as it slowly equilibrates. In our experiments we have to terminate the etching reaction after a certain period of time and we observe that the nanospheres continue to shrink as long as the reactants are present (Figure 1b), so we do not assume that the system in fact reaches an equilibrium state.

The probability of removal of an atom from the crystal is calculated similarly:

$$W_{n \rightarrow n-1} = min\left(1, \frac{\Lambda^3 n}{X V_{acc}}e^{\left(-\mu - \frac{\Delta E_{n-1,n}}{k_B T}\right)}\right) \qquad (S3)$$

where in this case $X = 10^9$ as before and $\Delta E_{n+1,n}$ represents the increase in energy due to breaking bonds between atoms by removing an atom from the crystal, plus a decrease in energy of 3.700 eV due to the chemical reaction. The results of a typical simulation run are shown in Supplementary Movie 1. Here we start with an octahedron of edge length 40 atoms for a total of 42,680 atoms. The brightness of each atom corresponds to its coordination number and therefore its energy. The vertices

are removed first, followed by the edges, and then the crystal gradually becomes more and more spherical as the original facets are slowly removed. This is also reflected in Figure S9, which shows how the number of atoms with different coordination numbers *CN* changes over the course of the simulation. Initially there are many atoms with $CN = 9$ on the faces of the octahedron and this number gradually diminishes as the faces are slowly removed. It takes roughly 10 million attempts at insertion or removal of atoms before all the atoms are etched away; the vast majority of attempts result in no change to the crystal at all. The simulation is this slow due to our large probability suppression factor, *X*.
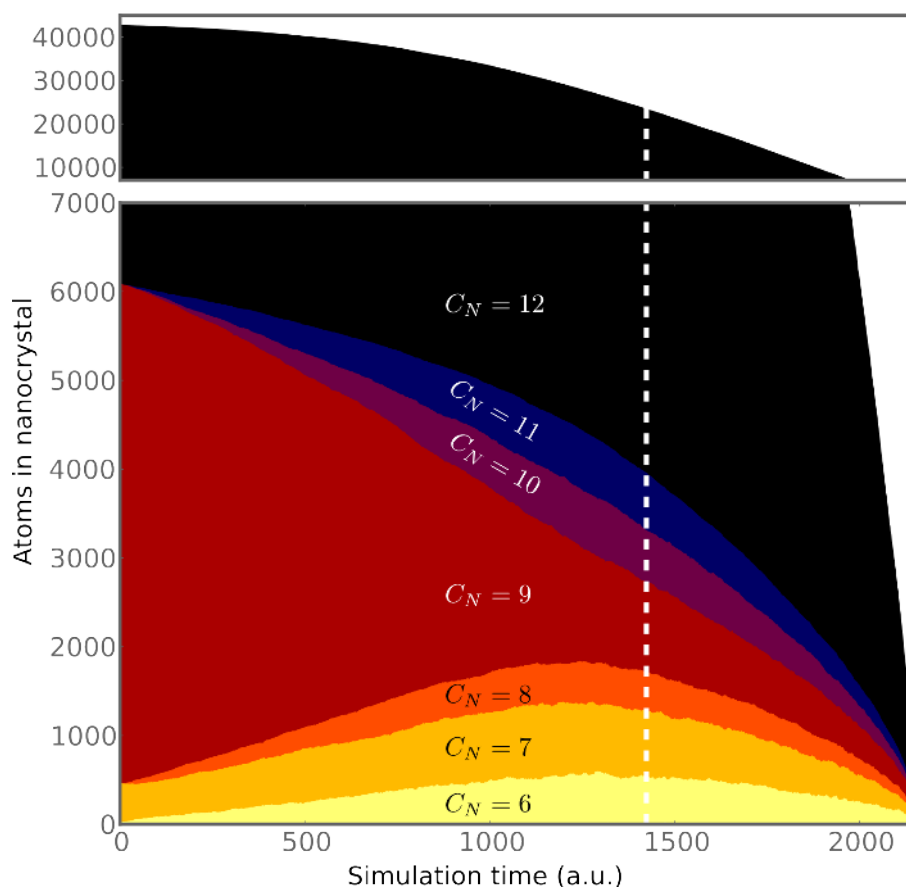

Figure S9. Number of atoms in a model octahedral nanocrystal as a function of etching simulation run time, color-coded by coordination number, C_N. The edge length is initially 40 atoms, or 42,680 atoms total. The percentage of atoms with $C_N < 6$ is negligible. The dashed white line marks the point when original faces of the octahedron have been completely removed. Until the very end of the simulation the majority of atoms are in the interior of the crystal with $C_N = 12$.

6. Comparison to citrate-stabilized gold nanoparticles

Citrate-stabilized gold nanoparticles were purchased from British Biocell International or BBI (100 nm), Strem Chemicals (90 nm), and Nano Partz (100 nm). Inspection of the particles with scanning electron microscopy (Figure S10) revealed that all three colloids consisted of faceted or lumpy particles which were not all the same size. Qualitatively, these micrographs show that these conventional gold nanoparticles are not perfectly spherical or monodisperse. We used one of these colloids (BBI, 100 nm diameter) for more thorough quantitative comparison with the spherical gold crystals.
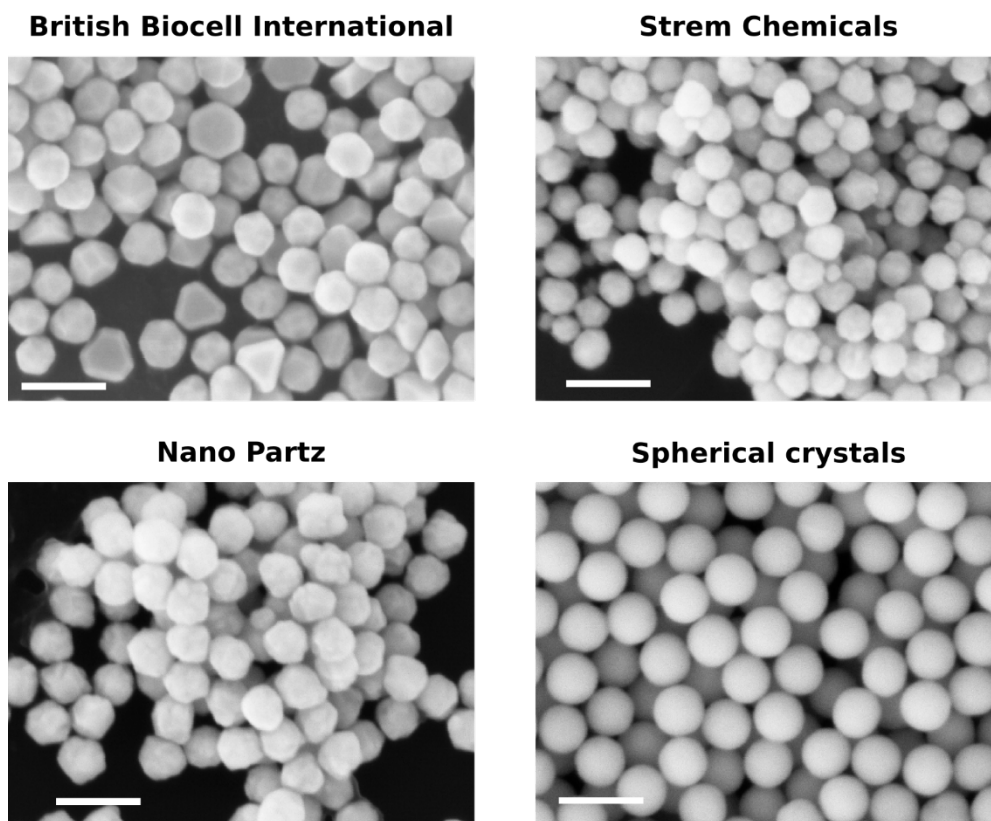
British Biocell International

Strem Chemicals

Nano Partz

Spherical crystals

Figure S10. Scanning electron micrographs of gold nanoparticles purchased from various suppliers and as prepared with the growth and etching technique described in this manuscript. Scale bars are 200 nm.

7. FDTD simulations of scattering spectra

We carried out finite-difference time-domain (FDTD) scattering simulations with a total-field scattered-field implementation[10] of the commercial software package Lumerical, version 6.5.11. Our simulation volume is 1 μm × 1.3 μm × 0.5 μm and our mesh for FDTD calculations consists of 1 nm^3 cubes. The grid boundaries in the simulation space are perfectly matching layers (PML).

Within this volume our model quadrumer is based on measurements of the experimental system's geometry. We simulated particles of diameter 130 nm, corresponding to measurements of our experimental quadrumer that we obtained with transmission electron microscopy. The simulated particles are embedded in a dielectric elliptical disc of major axis 174 nm, minor axis 126 nm, and depth 60 nm. The refractive index of this disc is 1.45. The particles embedded in this disc are separated from each other by gaps of 1.5 nm. The Formvar substrate is not modeled in the simulation. The simulated particles are large enough compared to the mesh size that surfaces in the simulation are relatively smooth. We verified that this mesh size was adequate by checking that the simulations converged in the near-infrared spectral region of interest even as we fine-tuned the mesh size. The simulated quadrumer, as rendered by Lumerical, can be seen in the images below.
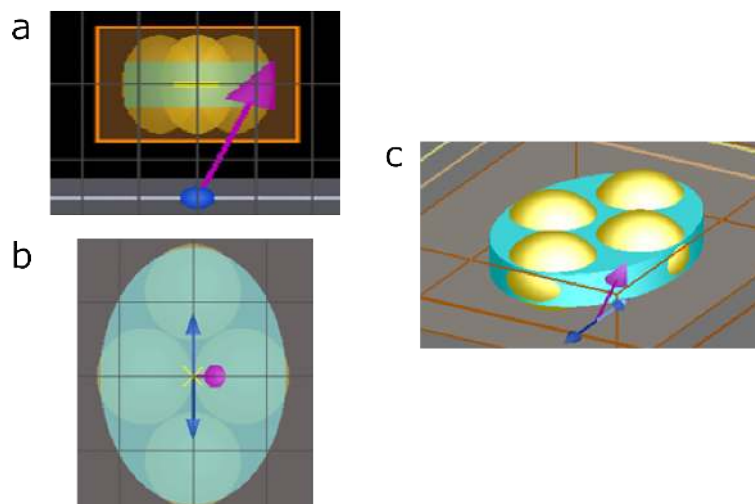
Figure S11. Rendering of a model quadrumer used for FDTD simulations, as viewed along the major axis (a), perpendicular to the plane of the axes (b), and at an angle (c). Gold spheres of diameter 130 nm are embedded in an elliptical disc of constant refractive index 1.45 (blue). Purple arrow indicates propagation direction of incident light and dark blue arrows indicate electric field orientation for 0° polarization.

An electromagnetic plane wave pulse is introduced, corresponding to a 700 nm – 1400 nm wavelength range. This plane wave propagates in a direction indicated by the purple arrow in Figure S11 for an angle of incidence of 20°, approximately the same angle of incidence that we used in the near-normal incidence dark-field spectroscopy technique. We obtained the scattering spectrum by collecting the power in the scattered field from a cone with a numerical aperture of 0.65, situated on the same side of the source as the spectrometer in our experimental system.

8. Discrepancies between experimental and simulated quadrumer scattering spectra

There are differences between the calculated and measured spectra of the quadrumer, especially at wavelengths shorter than about 900 nm. As discussed in a previous report,[11] these discrepancies arise due to scattering from parts of the sample that are not modeled in the simulation. This includes interactions between the cluster and the thin Formvar substrate as well as scattering from other particles or TEM grid bars that are close to the quadrumer.

Another reason for differences between the simulated and experimental scattering spectra is inhomogeneous changes in the Formvar substrate due to beam damage from the TEM that is used to locate the cluster. TEM images of quadrumers that have already been imaged at higher magnification show circular patterns of beam damage, as shown in Figure S12. The electron beam can warp the Formvar or even puncture it. Combined with local heating from the metal nanoparticles, this may result in inhomogeneous variations in the substrate geometry or even the contact angle between the substrate and the nanoparticles. Beam damage to the substrate may result in variations in its refractive index that are not captured in the simulations either.
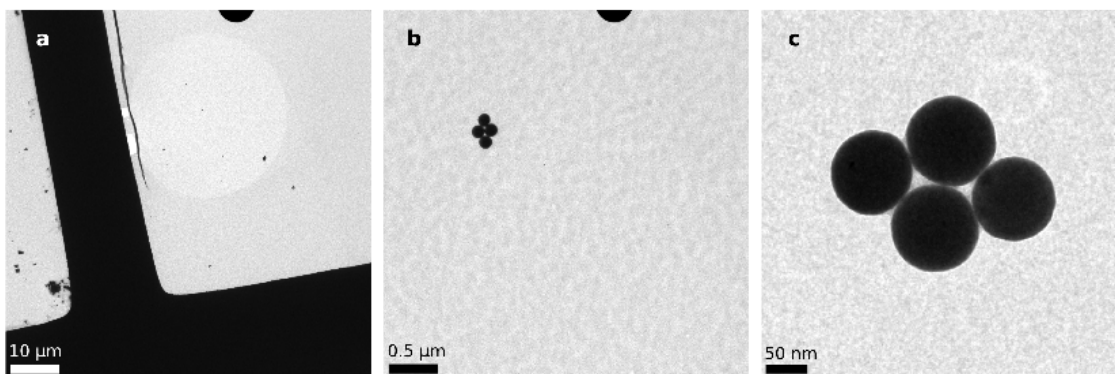
Figure S12. Transmission electron micrographs of quadrumer clusters of spherical gold crystals. (**a**) A low magnification image shows evidence of beam damage due to previous high magnification work on the same part of the sample. There is a circular region of beam damage which appears brighter in the image and a dark crease in the Formvar running parallel to a grid bar. (**b**) Higher magnification image of a quadrumer reveals the inhomogeneous nature of the Formvar substrate over a length scale of 100 nm. (**c**) High magnification image of a quadrumer shows material in the gaps between the particles, which causes the edges of the particles at the center of the cluster to appear blurry.

A layer of material is observed surrounding the nanoparticles in a cluster under TEM. It is unclear whether this is a consequence of beam damage or simply material that adsorbs to the particles during or before TEM sample preparation. The elliptical disc of dielectric material in the simulation is meant to model this layer, but its refractive index is treated as a fitting parameter. Our simulation models neither the exact morphology of this layer nor potentially inhomogeneous variations in the refractive index within it.

References

1. Li, C.; Shuford, K. L.; Chen, M.; Lee, E. J.; Cho. S. O. A Facile Polyol Route to Uniform Gold Octahedra with Tailorable Size and Their Optical Properties. *ACS Nano* **2008**, *2*, 1760–1769.
2. Rodríguez-Fernández, J.; Pérez-Juste, J.; Mulvaney, P.; Liz-Marzán, L. M. Spatially-Directed Oxidation of Gold Nanoparticles by Au(III)-CTAB Complexes. *J. Phys. Chem. B* **2005**, *109*, 14257–14261.
3. Torigoe K.; Esumi, K. Preparation of Colloidal Gold by Photoreduction of Tetracyanoaurate (1-)-Cationic Surfactant Complexes. *Langmuir* **1992**, *8*, 59–63.
4. Seo, D.; Park, J. C.; Song, H. Polyhedral Gold Nanocrystals with O_h Symmetry: From Octahedra to Cubes. *J. Am. Chem. Soc.* **2006**, *128*, 14863–14870.
5. Barnard, A. S.; Lin, X. M.; Curtiss, L. A. Equilibrium Morphology of Face-Centered Cubic Gold Nanoparticles >3 nm and the Shape Changes Induced by Temperature. *J. Phys. Chem. B* **2005**, *109,* 24465–24472.
6. Foiles, S. M.; Baskes, M. I.; Daw, M. S. Embedded-Atom-Method Functions for the FCC Metals Cu, Ag, Au, Ni, Pd, Pt, and Their Alloys. *Phys. Rev. B* **1986**, *33,* 7983–7991.
7. Metropolis, N.; Rosenbluth, A. W.; Rosenbluth, M. N.; Teller, A. H.; Teller, E. Equation of State Calculations by Fast Computing Machines. *J. Chem. Phys.* **1953**, *21*, 1087–1092.
8. Frenkel, D.; Smit, B. *Understanding Molecular Simulation: From Algorithms to Applications*; Academic Press: San Diego, 2001; pp 126-135.
9. Mariscal, M. M.; Velázquez-Salazar, J. J.; Yacaman, M. J. Growth Mechanism of Nanoparticles: Theoretical Calculations and Experimental Results. *CrystEngComm* **2012**, *14*, 544-549.
10. Taflove, A.; Hagness, S. C. *Computational Electrodynamics: The Finite-Difference Time-Domain Method*; Artech House: Boston, 2000.
11. Fan, J. A.; Wu, C.; Bao, K.; Bao, J.; Bardhan, R.; Halas, N. J.; Manohanran, V. N.; Nordlander, P.; Shvets, G.; Capasso, F. Self-Assembled Plasmonic Nanoparticle Clusters. *Science* **2010**, *328*, 1135–1138.